Hu, P. *et al*. (2015) ***Géotechnique Letters* 5**, 131–139, http://dx.doi.org/10.1680/jgele.15.00051

A comparison of full profile prediction methods for a spudcan penetrating sand overlying clay

P. HU*, S. A. STANIER*, D. WANG* and M. J. CASSIDY*

Spudcans are the traditional footings used for offshore mobile jack-up rigs. However, the installation of spudcans in sand overlying clay may lead to punch-through failure, which can cause serious damage to the jack-up rig and endanger personnel. This article compares three new methods proposed in the literature and an interpretation of the International Organization for Standardization (ISO) guideline for predicting the full penetration resistance profile. The penetration resistance profile for each of the methods is characterised by two key calculations: the peak resistance in the sand and the bearing capacity within the underlying clay. The punch-through distance – an indicator of the potential for and severity of punch-through failure – is estimated from these calculations. In comparison with 71 geotechnical centrifuge tests, the ISO guideline provides poor predictions, consistently underestimating the peak resistance in the sand and the underlying bearing capacity in the clay. Although all three of the new methods provide a superior response, by assessing the accuracy, scatter and geometric skew of the predictions, two of the methods are shown to be biased in at least one of the key calculations used to define the penetration resistance profile, thus producing bias in the prediction of the punch-through distance. However, one method yields largely unbiased predictions.

KEYWORDS: bearing capacity; centrifuge modelling; footings/foundations; offshore engineering

NOTATION

A	widest cross-sectional area of spudcan
D	diameter of spudcan
D_F	distribution factor
d	penetration depth of spudcan
d_{base}	depth from bottom of sand plug to sand–clay interface
d_c	depth factor
d_{peak}	spudcan depth at peak penetration resistance
d_{punch}	punch-through distance
$d_{punch,calculated}$	calculated punch-through distance
$d_{punch,measured}$	measured punch-through distance
d_{sb}	depth from bottom of sand plug to soil surface
E^*	parameter to simplify algebra
H_{eff}	distance between depth of peak resistance and sand–clay interface
H_{fdn}	height of composite foundation of spudcan and sand plug
H_{plug}	sand plug height
H_s	sand thickness
h_f	thickness of spudcan at widest section
I_D	relative density
K_p	coefficient of passive earth pressure
K_s	punching shear coefficient
k	strength gradient of clay
N_c	bearing capacity factor
N_{c0}	bearing capacity factor of clay at base level of a circular foundation
$N_{c,calculated}$	calculated bearing capacity factor
$N_{c,measured}$	measured bearing capacity factor
n_s	load spread factor
$Q_{c,peak}$	clay vertical bearing capacity subjected to vertical and inclined loadings within an area of radius R
$Q_{s,peak}$	vertical component of shear force developed along a simplified inclined failure surface in the upper sand layer
Q_v	bearing capacity in clay
q_0	effective overburden pressure
q_{clay}	penetration resistance in the clay layer
q_{peak}	peak penetration resistance
$q_{peak,calculated}$	calculated peak penetration resistance
$q_{peak,measured}$	measured peak penetration resistance
r	geometric parameter
s_c	shape factor
s_u	undrained shear strength of clay
s_{u0}	clay shear strength at lowest level of the spudcan widest cross-sectional area
s_{ua}	average value of shear strength from $d - h_f$ to $d + H_{plug}$
s_{ub}	shear strength of clay at base of composite foundation
s_{um}	shear strength of clay at sand–clay interface
V_f	volume of spudcan
W_{peak}	weight of sand wedge trapped between spudcan level and sand–clay interface
α_{side}	side adhesion factor
γ'_c	effective unit weight of clay
γ'_s	effective unit weight of sand
θ^*	skew angle
κ	dimensionless strength increasing parameter for non-homogeneous cohesive soils
σ	standard deviation
ϕ_2	reduced operative friction angle
ϕ'	friction angle of sand
ϕ^*	reduced friction angle due to non-associated flow rule
ϕ_{cv}	critical state friction angle of sand
ψ	dilation angle of sand
ω	geometric parameter

Manuscript received 31 March 2015; first decision 7 May 2015; accepted 21 May 2015.
Published online at www.geotechniqueletters.com on 10 August 2015.
*Centre for Offshore Foundation Systems and ARC Centre of Excellence for Geotechnical Science and Engineering, The University of Western Australia, Crawley, WA, Australia

INTRODUCTION

Offshore jack-ups typically consist of a buoyant triangular hull supported by three independent legs that are fitted with spudcan foundations (Fig. 1). Punch-through events can occur during installation in sand overlying clay when the sand layer yields, causing the spudcan to plunge into the underlying weaker clay. A large number of centrifuge model tests investigating punch-through in sand overlying clay have been reported (Lee, 2009; Teh *et al.*, 2010; Lee *et al.*, 2013a; Hu *et al.*, 2014a; Hu, 2015). Retrospective predictions for this database of experiments are used to assess and compare punch-through predictions from the latest industry guidelines for the site-assessment of jack-ups (ISO, 2012) and three new methods, proposed by

- Teh (Teh, 2007)
- Lee *et al.* (Lee, 2009; Lee *et al.*, 2013a, 2013b)
- Hu *et al.* (Hu *et al.*, 2014a, 2014b; Hu, 2015).

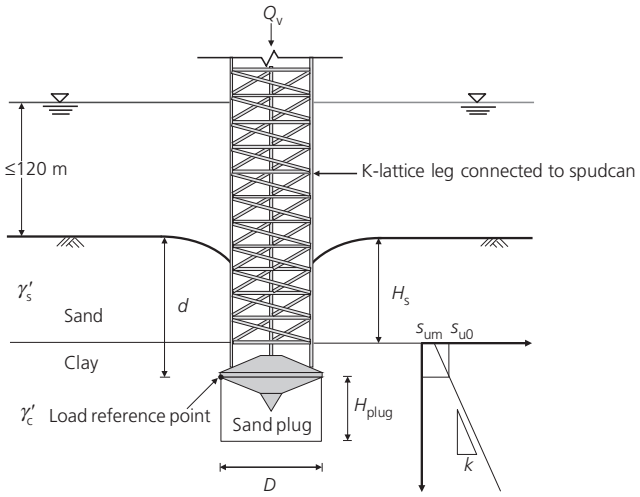

Fig. 1. Problem definition and notation

SIMPLIFIED FULL PROFILE PREDICTION

All four methods simplify the spudcan penetration profile (Fig. 2) as a combination of

- A, spigot embedment resistance
- B, peak resistance in the sand layer q_{peak}
- C, resistance at the sand–clay interface and
- D, resistance in the clay layer q_{clay} where it is equal to q_{peak}.

The punch-through distance is assessed by calculating the depth over which q_{peak} is greater than q_{clay}. Table 1 provides all of the design equations used to generate the predictions, with Figs 3 and 4 showing the basis of the calculations.

Peak resistance

In the method proposed by Teh, q_{peak} is composed of the vertical component of the shearing resistance in the mobilised sand frustum, the bearing capacity of the underlying clay and the self-weight of the sand. However, the full bearing capacity of the underlying clay is assumed to act on a limited region from the centreline, beyond which the bearing capacity is assumed to reduce linearly to a minimum value of $0{\cdot}5q_{clay}$ (Fig. 3(a)).

The Lee *et al.* method assumes that q_{peak} occurs when a sand frustum with a dispersion angle equal to the mobilised dilation angle of the sand is pushed into the underlying clay; q_{peak} is the sum of the frictional resistance in the sand, the bearing capacity of the underlying clay and the weight of the sand frustum (Fig. 3(b)).

The Hu *et al.* method modifies the method of Lee *et al.* to account for the embedment depth attained during the mobilisation of q_{peak} (Fig. 3(c)) and extends it to account for various spudcan geometries and sand densities. The relationship for a distribution factor D_F was optimised for the new mechanism, resulting in power relationships calibrated for both very dense and medium-dense sands and for footing conical angles from 0° to 21° (Hu *et al.*, 2014a; Hu, 2015).

In application of the three methods in this article, the depth of the peak resistance d_{peak} is taken as $0{\cdot}12H_s$ (when $0{\cdot}16 \leq H_s/D \leq 1$), where H_s is the sand layer thickness and

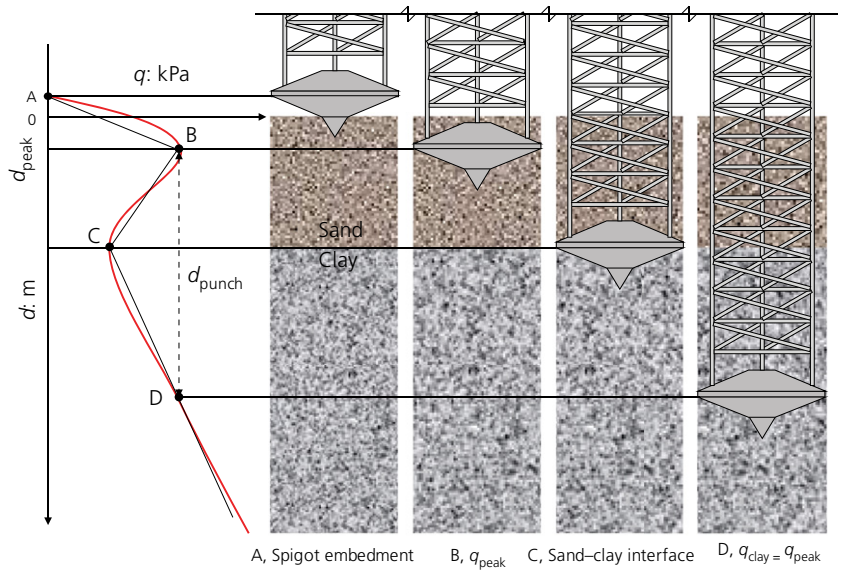

Fig. 2. Simplified spudcan penetration resistance profile prediction method

Table 1. Full profile design equations for the Teh method, Lee *et al*. method, ISO methods and Hu *et al*. method

Method	
Teh method (Teh, 2007)	
$q_{peak}=\frac{Q_{s,peak}+Q_{c,peak}-W_{peak}}{A}$	(1)
$Q_{s,peak}=\frac{\pi\gamma'_s K_p \sin(\phi_2-\omega)}{\cos\phi_2\cos\omega}\left[\left(d_{peak}+\frac{1}{2}H_{eff}\right)DH_{eff}+d_{peak}\tan\omega H_{eff}^2+\frac{2}{3}\tan\omega H_{eff}^3\right]$	(2)
$Q_{c,peak}=\pi(N_c s_{um}+H_s\gamma'_s)\left[R^2-\frac{0{\cdot}5}{R-r}\left(\frac{2}{3}R^3+\frac{1}{3}r^3-R^2r\right)\right]$	(3)
$W_{peak}=\frac{1}{3}\pi H_{eff}\left[\left(\frac{D}{2}\right)^2+R\frac{D}{2}+R^2\right]\gamma'_s$	(4)
$q_{clay}=s_{ub}N_c+\frac{4s_{ua}\alpha_{side}(H_{plug}+h_f)}{D}+\frac{\gamma'_c V_f}{A}$	(5)
$N_c=10\left(1+\ 0{\cdot}075\frac{d+H_{plug}}{D}\right)$	(6)
Lee *et al*. method (Lee, 2009; Lee *et al*., 2013a, 2013b)	
$q_{peak}=(N_{c0}s_{um}+q_0)\left(1+\frac{2H_s}{D}\tan\psi\right)^{E^*}+\frac{\gamma'_s D}{2\tan\psi(E^*+1)}\left[1-\left(1-\frac{2H_s}{D}E^*\tan\psi\right)\left(1+\frac{2H_s}{D}\tan\psi\right)^{E^*}\right]$	(7)
$N_{c0}=6{\cdot}34+0{\cdot}56\frac{k(D+2H_s\tan\psi)}{s_{um}}$	(8)
$E^*=2\left[1+D_F\left(\frac{\tan\phi^*}{\tan\psi}-1\right)\right]$	(9)
$D_F=0{\cdot}726-0{\cdot}219\frac{H_s}{D}\ \ \left(\frac{H_s}{D}\le 1{\cdot}12\right)$	(10)
$D_F=1{\cdot}333-0{\cdot}889\frac{H_s}{D}\ \ \left(\frac{H_s}{D}\le 0{\cdot}9\right)$	(11)
$\tan\phi^*=\frac{\sin\phi'\cos\psi}{1-\sin\phi'\sin\psi}$	(12)
$q_{clay}=N_c s_{ub}+\gamma'_c H_{fdn}$	(13)
$N_c=4\frac{d_{base}}{D}+9$ as $\frac{d_{base}}{D}\ge\frac{H_{fdn}}{D}$	(14)
$N_c=\left(1-\frac{0{\cdot}5\kappa(H_{fdn}/D)}{1+\kappa(d_{base}/D)}\right)\left[18{\cdot}2\left(\frac{H_{fdn}}{D}+0{\cdot}7\right)^{1/2}-2\right]$ as $\frac{H_{fdn}}{D}\le 1{\cdot}12$ and $\frac{d_{base}}{D}>\frac{H_{fdn}}{D}+0{\cdot}5$, where $\kappa=kD/s_{um}$	(15)
$q_{clay}=N_c s_{ub}+\gamma'_c H_{fdn}$	(16)
ISO methods (ISO, 2012) Load spread method	
$q_{peak}=\left(1+2\frac{H_s}{n_s D}\right)^2(s_u N_c s_c d_c-\gamma'_s H_s)$	(17a)
$q_{peak}=\left(1+2\frac{H_s}{n_s D}\right)^2 s_u N_c s_c d_c$	(17b)
Punching shear method	
$q_{peak}=(s_u N_c s_c d_c+q_0)-H_s\gamma'_s+2\frac{H_s}{D}(H_s\gamma'_s+2q_0)K_s\tan\phi'$	(18a)
$q_{peak}=(s_u N_c s_c d_c+q_0)+2\frac{H_s}{D}(H_s\gamma'_s+2q_0)K_s\tan\phi'$	(18b)
Penetration resistance in clay	
$q_{clay}=s_u N_c s_c d_c+q_0$	(19)
Hu *et al*. method (Hu *et al*., 2014a, 2014b; Hu, 2015)	
$q_{peak}=(N_{c0}s_{um}+q_0+0{\cdot}12\gamma'_s H_s)\left(1+\frac{1{\cdot}76H_s}{D}\tan\psi\right)^{E^*}+\frac{\gamma'_s D}{2\tan\psi(E^*+1)}\left[1-\left(1-\frac{1{\cdot}76H_s}{D}E^*\tan\psi\right)\left(1+\frac{1{\cdot}76H_s}{D}\tan\psi\right)^{E^*}\right]$	(20)
$N_{c0}=6{\cdot}34+0{\cdot}56\frac{k(D+1{\cdot}76H_s\tan\psi)}{s_{um}}$	(21)
$E^*=2\left[1+D_F\left(\frac{\tan\phi^*}{\tan\psi}-1\right)\right]$	(22)

Continued

Table 1 *Continued*

Method	
$D_F = 0{\cdot}642\left(\frac{H_s}{D}\right)^{-0{\cdot}576}$ as $0{\cdot}16 \leq \frac{H_s}{D} \leq 1{\cdot}0$	(23)
$D_F = 0{\cdot}623\left(\frac{H_s}{D}\right)^{-0{\cdot}174}$ as $0{\cdot}21 \leq \frac{H_s}{D} \leq 1{\cdot}12$	(24)
$\tan\phi^* = \frac{\sin\phi'\cos\psi}{1-\sin\phi'\sin\psi}$	(25)
$q_{clay} = N_c s_{u0} + H_{plug}\gamma'_c = N_c s_{u0} + 0{\cdot}9H_s\gamma'_c \left(0{\cdot}16 \leq \frac{H_s}{D} \leq 1{\cdot}00\right)$	(26)
$N_c = 11\frac{H_s}{D} + 10{\cdot}5\left(0{\cdot}16 \leq \frac{H_s}{D} \leq 1{\cdot}12\right)$	(27)

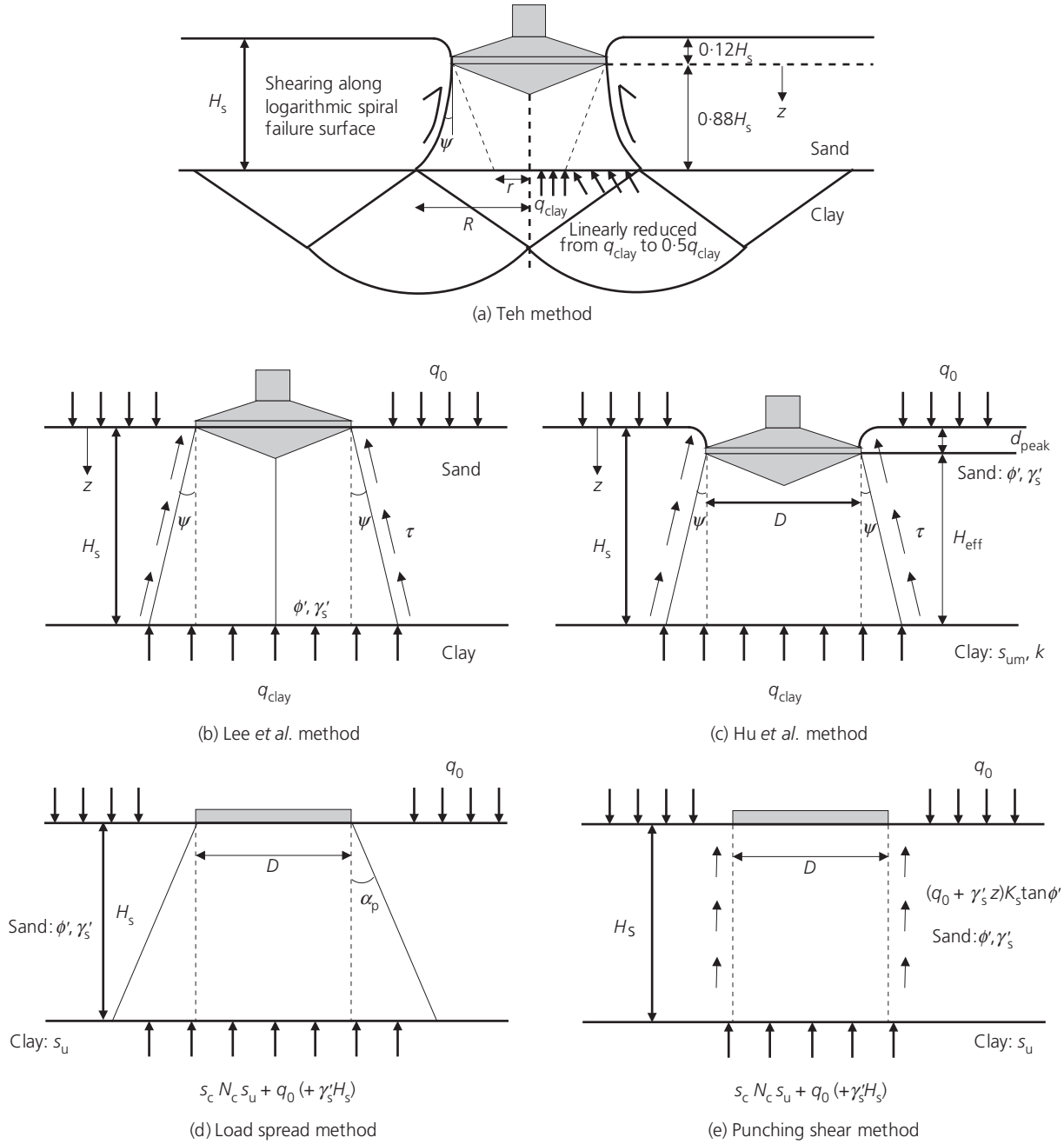

Fig. 3. Conceptual models for peak resistance from methods of (a) Teh, (b) Lee *et al*., (c) Hu *et al*., (d) load spread method of ISO and (e) punching shear method of ISO

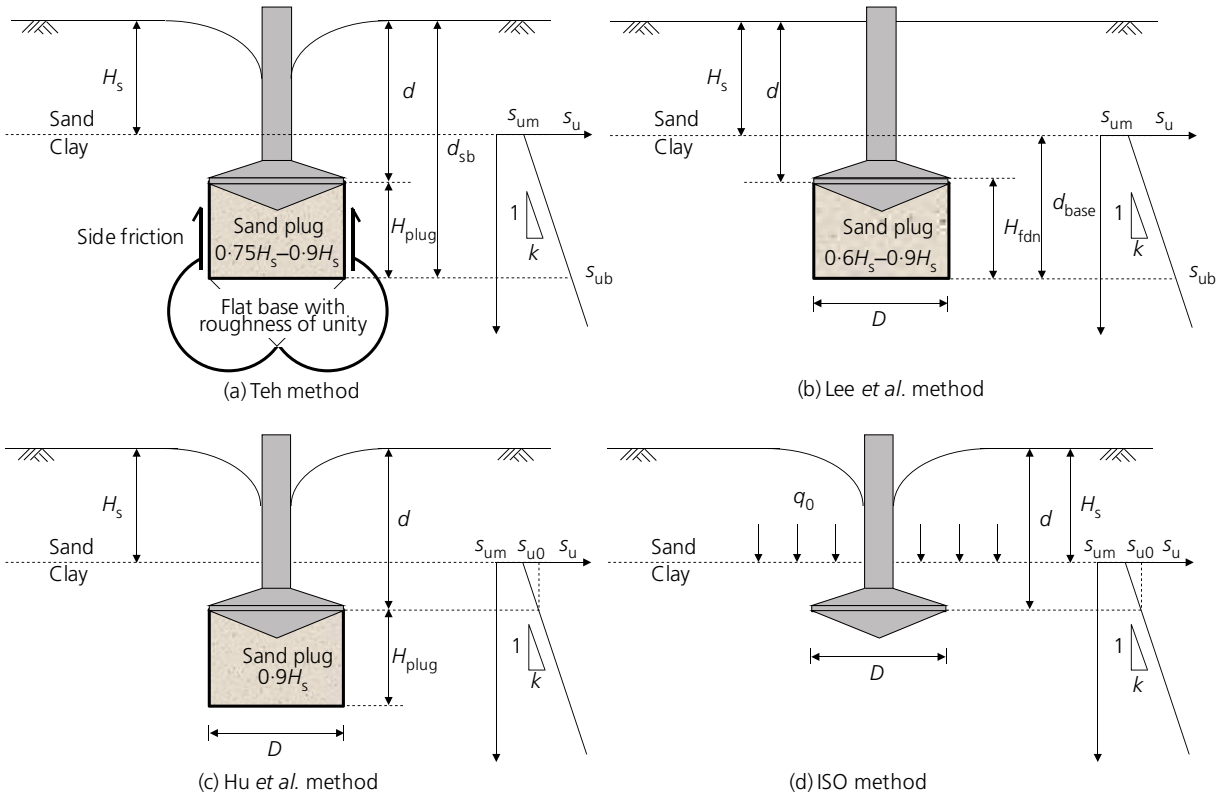

Fig. 4. Nomenclature of soil bearing capacity in underlying clay for methods of (a) Teh, (b) Lee *et al*., (c) Hu *et al*. and (d) ISO

Table 2. Summary of sand overlying clay centrifuge tests reported in the literature

	Lee (2009) UWA tests	Teh *et al*. (2010) NUS tests	Teh *et al*. (2010) UWA tests	Lee *et al*. (2013a) UWA tests	Hu *et al*. (2014a) UWA tests	Hu (2015) UWA tests	Summary
Centrifuge type	Beam	Beam	Beam	Drum	Drum	Drum	Beam/drum
Number of tests	5	7	3	30	15	11	71
Geometry							
D: m	8–14	10	4–8	6–16	6–20	8	4–20
H_s: m	7	3–10	3·5–7·1	3·4–6·7	3·2–6	3·03–7·25	3–10
H_s/D	0·50–0·88	0·3–1·0	0·58–0·89	0·21–1·12	0·16–1·00	0·38–0·91	0·16–1·12
Conical angle: degrees	13	10	13	0–13	13	0–21	0–21
Sand							
I_D: %	99	58–95	98–99	92	43	74	43–99
ϕ_{cv}: degrees[a]	31	32	31	31	31	31	31–32
γ'_s: kN/m^3	11·15	9·15–9·93	11·13–11·15	10·99	9·96	10·61	9·15–11·15
Clay[b]							
s_{um}: kPa	13·2	7·75–25·82	7·22–14·62	16·3–19·1	11·01–12·96	11·31–22·24	7·22–25·82
k: kPa/m	1·85	1·56	1·20	2·10	1·54–1·55	1·51–2·13	1·2–2·13
γ'_c: kN/m^3	N/A	6	6·5	7·5	7·11	7·21	6–7·5
Results							
q_{peak}: kPa	421·30–606·48	154·78–699·54	270–608	219–712	169·92–382·95	237·28–758·95	154·78–758·95
d_{punch}: m	N/A	3·93–7·30	9·16–10·33	0·20–12·20	5·22–8·10	4·75–13·94	0·20–13·94

[a]ϕ_{cv} is the critical state friction angle of sand
[b]Kaolin clay was used in all the centrifuge tests

D is the diameter of the spudcan. This is based on experimental observations of Teh *et al*. (2008, 2010) and Hu *et al*. (2014a).

ISO (2012) recommends both load spread and punching shear methods. For the load spread method (Fig. 3(d)), q_{peak} is equated to the capacity of a fictitious footing of increased area at the sand–clay interface (a load spread ratio of 3 is used as it provides higher q_{peak} predictions). However, there is ambiguity regarding the position of the surcharge during the calculation of the bearing capacity of the larger fictitious footing. The ISO guideline (figure A9·3-11 of ISO 19905·5 (ISO, 2012)) indicates that the effective overpressure at the footing level should be used in conjunction with the bearing capacity equation (equation A9·3-7). In this case, the pressure should remain as just q_0 when calculating the bearing capacity of the fictitious footing. However, the authors consider that the actual surcharge on the clay layer should be assumed. That is, the surcharge at the spudcan

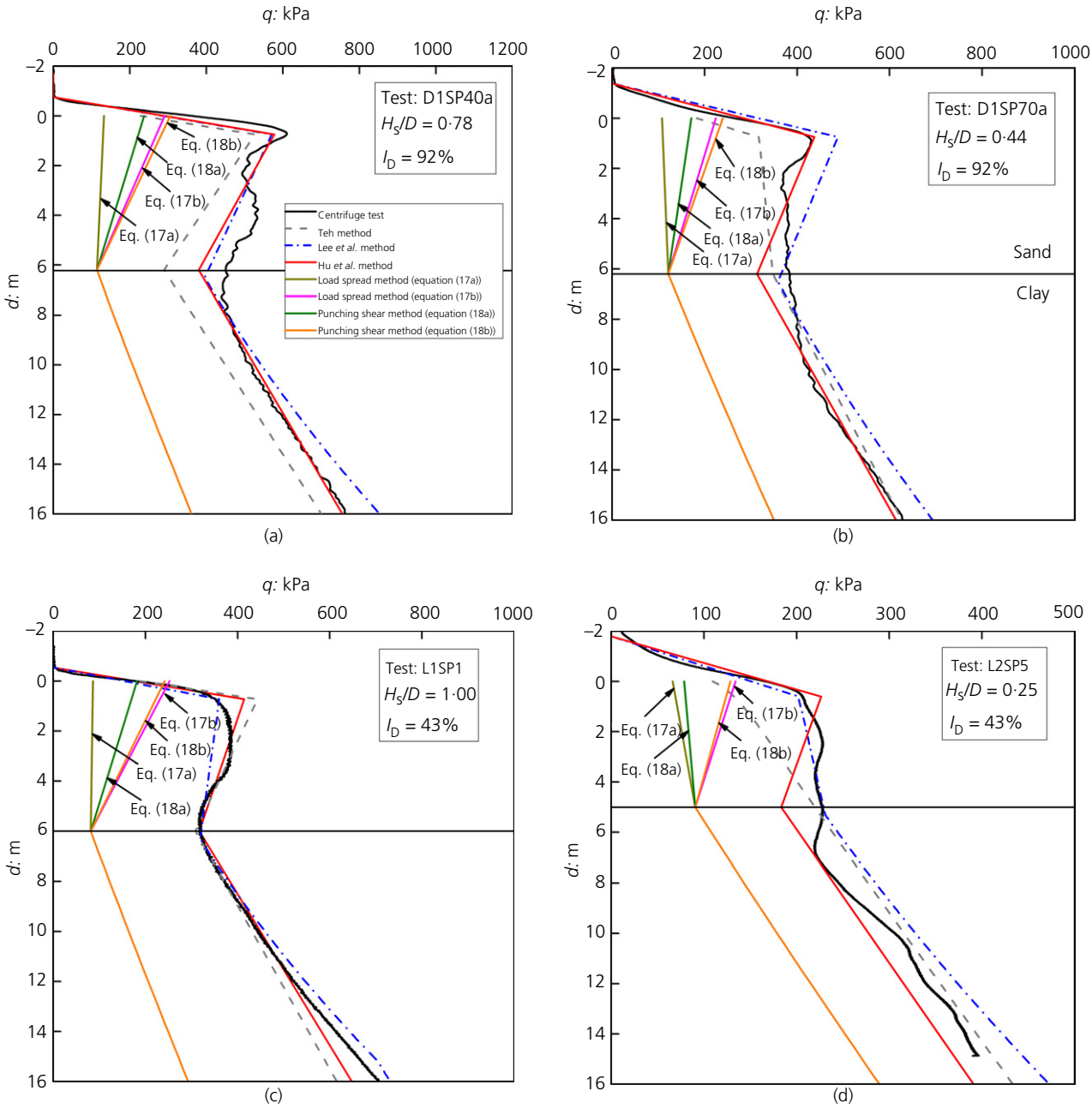

Fig. 5. Selected comparisons of experimentally measured punch-through profiles with all calculation methods

level (q_0) should have an additional surcharge due to the sand layer between it and the fictitious footing added to it (i.e. $q_0+\gamma'_s H_s$, where γ'_s is submerged unit weight of sand). Both assumptions were used to retrospectively predict the experimental database (equations (17a) and (17b) in Table 1).

The punching shear method (Fig. 3(e)) of ISO (2012) assumes that a cylindrical frustum of sand is pushed into the underlying clay, mobilising frictional resistance on the vertical surface of the frustum and clay bearing capacity at the base. This method has the same ambiguity as the load spread method regarding the position of the surcharge and therefore both assumptions were calculated (equations (18a) and (18b) in Table 1).

Clay resistance

All methods use a form of the bearing capacity equation to calculate spudcan resistance in the underlying clay layer, though with differing interpretations of the bearing capacity factor (N_c) and the influence of the sand plug that has been shown to become trapped beneath the spudcan (Craig & Chua, 1990; Teh *et al.*, 2008; Lee *et al.*, 2013a).

All three new methods assume that the entrapped sand plug is cylindrical in shape (Figs 4(a)–4(c)), though a range of sand plug heights from $0{\cdot}6H_s$ to $0{\cdot}9H_s$ was measured. A sand plug height of $0{\cdot}9H_s$ was concluded from both full-spudcan and half-spudcan centrifuge tests and further validated by large-deformation finite-element (FE) analyses in Hu (2015). To fairly compare the three methods, a value of $0{\cdot}9H_s$ was used in the retrospective predictions. ISO (2012) does not mention a sand plug and therefore none is assumed.

The Teh method uses the N_c factor derived by Hossain *et al.* (2006) for just a spudcan penetrating into a single clay layer. The Lee *et al.* method uses new N_c relations derived from small-strain FE analyses, accounting for the composite spudcan and sand plug. Alternatively, the Hu *et al.* method simplifies N_c by using an expression back-calculated from

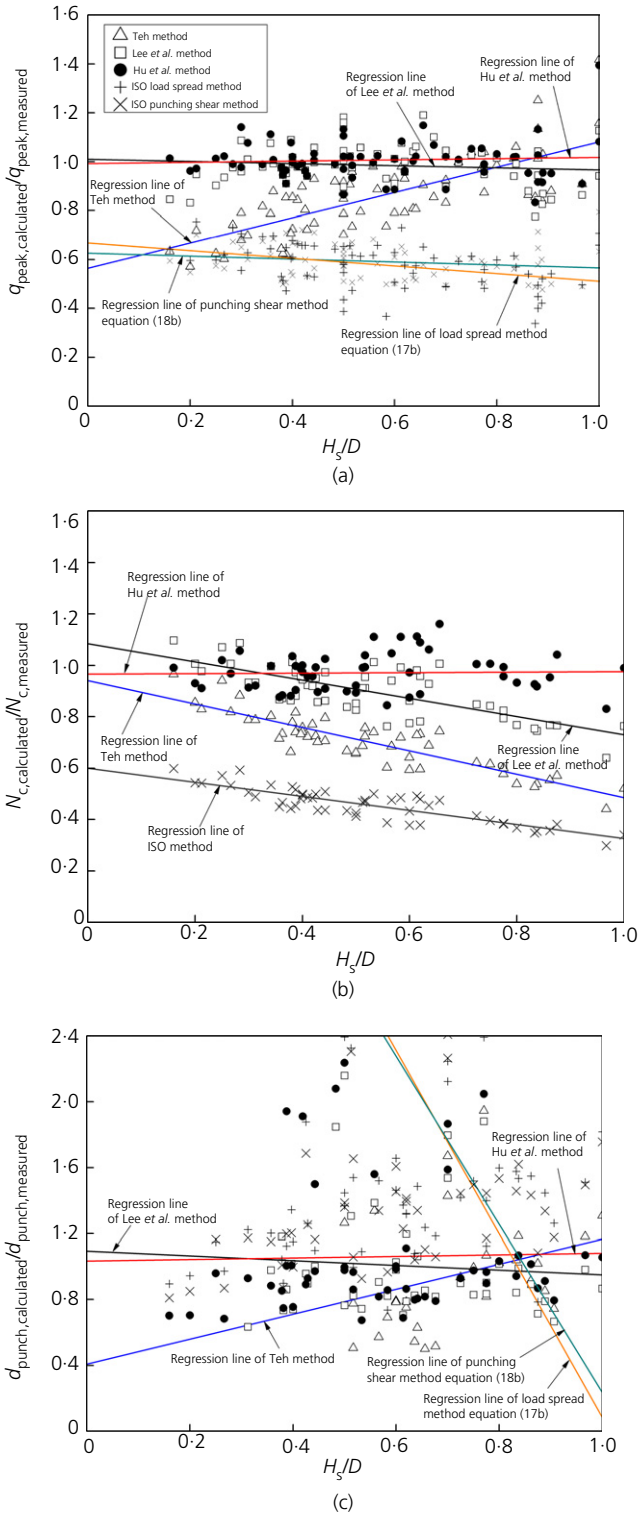

Fig. 6. Comparison of performance of calculation methods against centrifuge database: (a) peak penetration resistance q_{peak}; (b) bearing capacity factor N_c; (c) punch-through distance d_{punch}

large-deformation FE analyses of the full penetration process. The ISO guideline uses the expressions for N_c given in Houlsby & Martin (2003), so those were adopted for the ISO predictions.

COMPARISON AND DISCUSSION

The 71 centrifuge tests contributing to the experimental database are detailed in Table 2. These cover the range of parameters and geometries typically encountered in the field. Punch-through was observed in 62 of the 71 tests.

Full penetration resistance profile predictions

The methods were evaluated using retrospective predictions of the centrifuge experiments. Four typical centrifuge tests – two very dense sand tests (relative density $I_D = 92\%$) from Lee *et al.* (2013a) and two medium-dense sand tests ($I_D = 43\%$) from Hu *et al.* (2014a) – are first highlighted here to evaluate the performance of each method. All comparisons are available in the supplementary data.

As shown in Fig. 5, both q_{peak} and q_{clay} predicted by the Teh method deviate from those measured, and no punch-through is predicted for some of the cases in which punch-through was observed in the experiments. The Lee *et al.* method overestimates q_{clay}, which causes underestimation of the punch-through distance. Due to the adoption of the load spread method or the punching shear method for the calculation of q_{peak} and the effect of the sand plug in the underlying clay layer being ignored, the ISO method underestimates the penetration resistances significantly. In contrast, the Hu *et al.* method displays better prediction of both q_{peak} and q_{clay}, leading to better overall predictions of the penetration resistance and the punch-through distance.

Comparisons of q_{peak}, N_c and d_{punch}

Comparisons of q_{peak}, N_c and d_{punch} predicted using each method are presented in Fig. 6. Ratios of calculated to measured values for each of the measures are plotted against H_s/D and a linear regression line for each method is displayed to highlight the skew of the prediction. A statistical summary is provided in Table 3.

For the ISO load spread and punching shear methods, the interpretation with the additional surcharge (equations (17b) and (18b)) was used in Fig. 6 as it was shown in Fig. 5 that it performs better. As shown in Fig. 6(a), both the load spread method and the punching shear method under-predict q_{peak} significantly, with mean values of 0·58 and 0·59, respectively. The load spread method could be made to fit the database by adjusting the spreading ratio n_s (see Table 1). Values required to fit the experimental data were back-calculated and are shown in Fig. 7 to fit the range $0{\cdot}91 \leq n_s \leq 2{\cdot}07$, with a mean of 1·42. This is far smaller than the range between 3 and 5 recommended in the ISO guideline. Baglioni *et al.* (1982) suggested that the load dispersion angle in the load spread method is equal to the friction angle of sand, which is equivalent to $1{\cdot}73 \leq n_s \leq 2{\cdot}75$ derived from tests on field soil samples. The range reported here is consistent with the above findings.

The Teh method provides a conservative prediction of q_{peak}, with $q_{peak,calculated}/q_{peak,measured}$ generally less than unity. The predicted q_{peak} values might be as low as 40% of the experimental measurements. A large variation of the predictions is indicated by a high coefficient of variation (CoV) of 18%. The Lee *et al.* method yields a significantly improved prediction, with $q_{peak,calculated}/q_{peak,measured}$ between 0·77 and 1·28, a mean value of 0·98 and a much-reduced CoV of 9·4%. However, both Fig. 6(a) and Table 3 indicate that mild bias exists with H_s/D with a skew angle of −4·01°. This is improved upon with the Hu *et al.* method, which provides reasonably good comparisons with $q_{peak,calculated}/q_{peak,measured}$ between 0·83 and 1·39, a mean value of 1·01 and the lowest scatter and skew of all the methods (8·2% and 1·47°, respectively).

Figure 6(b) shows that the adoption of N_c values for spudcan penetration in single-layer clay causes significant under-prediction of N_c in the Teh and ISO methods,

Table 3. Model performance indicators for each of the prediction methods

	Teh method	Lee *et al.* method	Hu *et al.* method	ISO load spread method		ISO punching shear method	
				Equation (17a)	Equation (17b)	Equation (18a)	Equation (18b)
$q_{peak,calculated}/q_{peak,measured}$							
Number of tests	71	71	71	71	71	71	71
Minimum	0·57	0·77	0·83	0·07	0·34	0·33	0·48
Maximum	1·42	1·28	1·39	0·53	0·75	0·65	0·79
Mean	0·86	0·98	1·01	0·29	0·58	0·44	0·59
σ	0·16	0·09	0·08	0·10	0·09	0·06	0·07
θ^*: degrees[a]	27·29	−4·01	1·47	−13·18	−8·93	2·30	−3·47
CoV: %	17·98	9·36	8·19	35·89	15·77	14·13	12·19
$N_{c,calculated}/N_{c,measured}$							
Number of tests [b]	54	54	54	54	54	54	54
Minimum	0·44	0·64	0·83	0·30	0·30	0·30	0·30
Maximum	0·97	1·10	1·16	0·60	0·60	0·60	0·60
Mean	0·69	0·89	0·97	0·45	0·45	0·45	0·45
σ	0·11	0·10	0·07	0·07	0·07	0·07	0·07
θ^*: degrees	−24·47	−19·55	0·61	−15·32	−15·32	−15·32	−15·32
CoV: %	16·49	11·65	7·70	15·66	15·66	15·66	15·66
$d_{punch,calculated}/d_{punch,measured}$							
Number of tests[c]	32	47	54	36	62	56	62
Minimum	0·50	0·63	0·67	0·49	0·74	0·61	0·81
Maximum	1·95	2·16	2·24	4·54	27·30	10·56	24·75
Mean	0·97	1·00	1·06	1·05	2·50	1·64	2·45
σ	0·34	0·34	0·39	0·75	3·90	1·56	3·60
θ^*: degrees	37·20	−8·20	2·71	−58·07	−79·83	−69·49	−78·92
CoV: %	35·50	33·60	36·54	71·96	155·89	95·54	146·95

[a]Skew angle θ^* is the arctangent of the gradient of the linear regression line (see Fig. 6)
[b]Only 54 tests available for N_c comparison (see Table 1 in supplementary data)
[c]In total 62 tests have d_{punch} values (see Table 1 in supplementary data). This row reflects the number of punch-through potential predicted from each method

worsening with increasing H_s/D. N_c should increase with H_s/D due to the larger entrapped sand plug and this bias is largely alleviated in the Lee *et al.* method because the composite footing and sand plug is accounted for explicitly. However, a certain amount of skew remains because the small-strain FE analyses, on which the N_c factors were based, did not account for the drag-down of softer near-surface sediments or strain softening. The large-deformation analyses performed by Hu *et al.* (2014b) accounted for both of these effects, resulting in better predictions of N_c across the full range of H_s/D.

Finally, the punch-through distances measured in the centrifuge tests were compared with the predicted values. Although 62 tests were predicted to experience punch-through failure based on the ISO load spread method, this is considered a coincidence as significant under-predictions of q_{peak} and N_c were observed in Fig. 5 and in the supplementary data. In addition, large scatter and skews are reflected, with a CoV of 155·9% and a skew angle of −79·83°. The situation was not improved for the ISO punching shear method, with a mean of 2·45 and corresponding CoV of 147%. The Teh method could only capture punch-through for 32 out of the 62 tests. Significant scatter was indicated by a CoV of 35·5%, while the minimum discrepancy of the punch-through distance was ~50%. The Lee *et al.* method performs reasonably well, but certain cases remain that produce significant overestimations of the punch-through distance. Due to more accurate predictions of both q_{peak} and N_c, the Hu *et al.* method predicts the majority of the punch-through cases (54 in total). The estimated punch-through distances are within ±20% for the majority of the cases, and the skew is the smallest of all the methods at 2·71°.

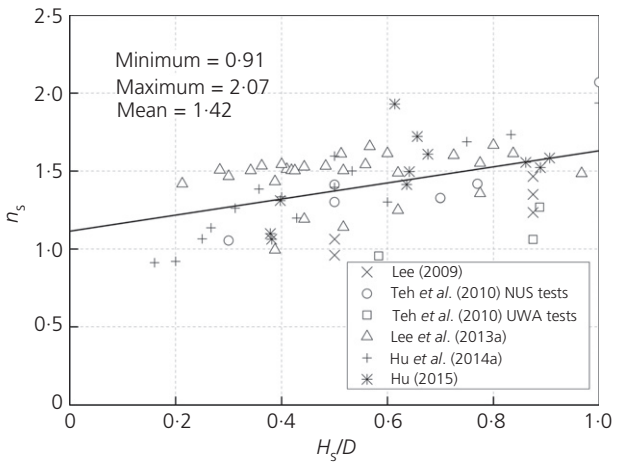

Fig. 7. Back-calculated n_s for the ISO load spread method to equal the experimentally measured q_{peak} (the additional surcharge of equation (17b) is considered); the legend references the experimental database

CONCLUSIONS

This article has assessed the performance of the ISO guideline and three new alternative methods for calculating the full resistance-penetration of a spudcan into sand overlying clay. The ISO method is shown to provide worryingly inaccurate predictions for a database of 71 tests. The Teh method shows skew in the q_{peak} and N_c predictions with respect to H_s/D. In certain cases, this results in the method erroneously indicating no potential for punch-through

failure. Although the Lee *et al*. method shows better performance overall, there is a certain amount of skew in the predictions with respect to H_s/D and, often, q_{peak} is well predicted while q_{clay} is poorly predicted or vice versa. The Hu *et al*. method shows the least skew with H_s/D, resulting in better predictions of q_{peak}, N_c and thus d_{punch}. The constructed penetration resistance profiles, which capture the distinctive aspects of a typical spudcan penetration resistance profile, are comparable with those obtained experimentally. The findings are valid within the range of experiments and simulations investigated here. Although the method has been tested on a comprehensive set of centrifuge tests, additional validation against field data would enhance confidence in its application.

ACKNOWLEDGEMENTS

This work forms part of the activities of the Centre for Offshore Foundation Systems (COFS), which is supported by the Lloyd's Register Foundation as a Centre of Excellence and currently forms one of the primary nodes of the Australian Research Council (ARC) Centre of Excellence for Geotechnical Science and Engineering. Lloyd's Register Foundation invests in science, engineering, and technology for public benefit, worldwide. This project received additional support from the Australia–China Natural Gas Technological Partnership Fund and the ARC Discovery program (DP1096764).

REFERENCES

Baglioni, V. P., Chow, G. S. & Endley, S. N. (1982). Jack-up foundation stability in stratified soil profiles. *Proc. 14th Offshore Technology Conf., Houston, TX*, OTC 4409.

Craig, W. H. & Chua, K. (1990). Deep penetration of spud-can foundation on sand and clay. *Géotechnique* **40**, No. 4, 541–556.

Hossain, M. S., Randolph, M. F., Hu, Y. & White, D. J. (2006). Cavity stability and bearing capacity of spudcan foundations on clay. *Proc. Offshore Technology Conf., Houston, TX*, OTC 17770.

Houlsby, G. T. & Martin, C. M. (2003). Undrained bearing capacity factors for conical footings on clay. *Géotechnique* **53**, No. 5, 513–520.

Hu, P. (2015). *Predicting punch-through failure of a spudcan on sand overlying clay.* PhD thesis, University of Western Australia, Perth.

Hu, P., Stanier, S. A., Cassidy, M. J. & Wang, D. (2014a). Predicting peak resistance of spudcan penetrating sand overlying clay. *J. Geotech. Geoenviron. Engng* **140**, No. 2, 04013009.

Hu, P., Wang, D., Cassidy, M. J. & Stanier, S. A. (2014b). Predicting the resistance profile of a spudcan penetrating sand overlying clay. *Can. Geotech. J.* **51**, No. 10, 1151–1164.

ISO (International Organization for Standardization) (2012). *ISO 19905-1: Petroleum and natural gas industries: site-specific assessment of mobile offshore unit*. 1: jack-ups. Geneva: ISO/FDIS.

Lee, K. K. (2009). *Investigation of potential spudcan punch-through failure on sand overlying clay soils.* PhD thesis, University of Western Australia, Perth.

Lee, K. K., Cassidy, M. J. & Randolph, M. F. (2013a). Bearing capacity on sand overlying clay soils: experimental and finite element investigation of potential punch-through failure. *Géotechnique* **63**, No. 15, 1271–1284.

Lee, K. K., Randolph, M. F. & Cassidy, M. J. (2013b). Bearing capacity on sand overlying clay soils: a simplified conceptual model. *Géotechnique* **63**, No. 15, 1285–1297.

Teh, K. L. (2007). *Punch-through of spudcan foundation in sand overlying clay.* PhD thesis, National University of Singapore, Singapore.

Teh, K. L., Cassidy, M. J., Leung, C. F., Chow, Y. K., Randolph, M. F. & Quah, M. (2008). Revealing the bearing capacity mechanisms of a penetrating spudcan through sand overlying clay. *Géotechnique* **58**, No. 10, 793–804.

Teh, K. L., Leung, C. F., Chow, Y. K. & Cassidy, M. J. (2010). Centrifuge model study of spudcan penetration in sand overlying clay. *Géotechnique* **60**, No. 11, 825–842.

WHAT DO YOU THINK?

To discuss this paper, please email up to 500 words to the editor at journals@ice.org.uk. Your contribution will be forwarded to the author(s) for a reply and, if considered appropriate by the editorial panel, will be published as a discussion.